Meridional Location of the Pacific Ocean Subtropical Gyre

RICHARD KLEEMAN

Courant Institute for Mathematical Sciences, New York, New York

NAOMI H. NAIK AND MARK A. CANE

Lamont-Doherty Earth Observatory, Palisades, New York

(Manuscript received 30 April 1998, in final form 17 September 1999)

ABSTRACT

The observed subtropical gyre in the North Pacific shows a shift in meridional location with depth. At shallow levels the density deviation peaks at around 15°N while at deep levels the peak is more like 30°N. It is argued here using analytical solutions to the beta-plane shallow-water equations that such a shift can be explained by the effects of oceanic dissipation processes. These solutions show that the highly damped solution is approximately proportional to Ekman pumping whereas the lightly damped case tends toward the classical Sverdrup solution. In the North Pacific, Ekman pumping peaks near 15°N while the Sverdrup solution peaks at 30°N. It is further demonstrated that 1) density deviations in the upper ocean are more highly influenced by higher order baroclinic modes than those in the deep, which are influenced by the lower modes, and 2) constant dissipation effectively acts much more strongly on the higher order baroclinic modes because of their slower speeds and smaller Rossby radii. These two factors thus explain the observed shift in the gyre with depth.

1. Introduction

Why are the subtropical gyres of the world oceans where they are? In his seminal work Sverdrup (1947) showed that the location of gyres was intimately related to the curl in the surface wind stress vector field. In particular the shift in the lower atmospheric easterlies of the tropics to the midlatitude westerlies was identified as the primary cause of the subtropical depression in the deep thermocline and an associated depth-averaged current gyre.

The observations in the Northern Pacific show, in fact, that this subtropical thermocline depression varies markedly with depth. Figure 1 displays a meridional section of density at 180° and shows that the minimum of density occurs at about 15°N for depths of the order of 100 m and at about 30°N for depths around 500 m. This deep gyre location[1] is in agreement with the Sverdrup solution.

The subtropical adjustment process towards the Sverdrup equilibrium solution was studied by Anderson and Gill (1975), who showed that the initial response to wind stress forcing is proportional to the local Ekman pumping and that the Sverdrup solution is only obtained after the arrival from the east of long Rossby waves. In a number of papers in the early 1980s[2] (Rhines and Young 1982a,b; Young and Rhines 1982) the issue of the vertical structure of this adjustment process was discussed. It was argued that in the case of the barotropic mode, the long Rossby waves are able to fully penetrate to the west and set up the Sverdrup solution. In the case of some baroclinic modes the Rossby wave speed may be of the same order or smaller than typical gyre currents and the authors suggest that this has the effect of ''shielding'' the gyre from baroclinic Rossby waves generated in the eastern basin. This is argued to occur by means of a refractive effect. Evidently such an ''incomplete'' Sverdrup adjustment process could, in principle, lead to vertical variation in the meridional location of the gyre as can indeed be seen in Rhines and Young's solutions.

The interaction of baroclinic modes with the mean state is currently an unresolved issue both observationally and theoretically. Early observational studies involving XBT data (see White et al. 1985 and references

[1] In this paper we define this to mean the latitude of the pressure or density extremum at a given depth in the ocean.

Corresponding author address: Dr. Richard Kleeman, Courant Institution for Mathematical Sciences, 251 Mercer Street, New York, NY 10012.
E-mail: kleeman@cims.nyu.edu

[2] A good summary of this material may be found in chapter 3 of Pedlosky (1996).

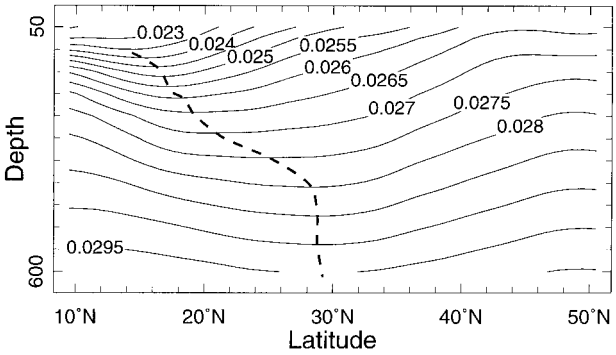

FIG. 1. A meridional section of density in the North Pacific at 180°. The dashed line shows the approximate latitude of minimal density for a given depth in the ocean. Units are g $cm^{-3} - 1$ and the data is derived from the annually averaged Levitus and Boyer (1994) climatology.

cited therein) found reasonable evidence for propagation of low-order, long-wave baroclinic Rossby waves across most of the basin at North Pacific subtropical latitudes. The phase speed of the diagnosed perturbations agreed reasonably with linear theory, which argued against a major interaction with the mean flow. More recently the TOPEX/Poseidon altimeter data has been analyzed by Chelton and Schlax (1996) (see also LeTraon and Minster 1993; Cipollini et al. 1997) who found that the phase speed of disturbances tended to be somewhat above that predicted by linear theory with this effect increasing with latitude and being of order 10% to 20% in the subtropics. The reason for this discrepancy is presently uncertain with authors such as Qiu et. al. (1997) suggesting that it is due to the observed perturbations being a combination of forced and free modes, while others such as Killworth et. al. (1997) and Dewar (1998) argue that the mean state tends to increase the wave speeds. The latter theoretical studies presented no evidence of a refractive effect, which agrees with earlier studies that used idealizations of observed currents (see Philander 1990, p. 150) to suggest that such an effect (involving a critical layer) may occur at 10° and 3°N but not at subtropical latitudes. It should be noted that these studies apply primarily to the first baroclinic mode, which for some parameter choices may not be highly refracted in the Rhines and Young theoretical framework. Evidently to resolve these issues, the interaction of higher-order baroclinic modes needs also to be addressed.

Given these uncertainties in the verification of this important aspect of the Rhines and Young theory, there seems grounds for considering a simpler explanation for the gyre location. In the present contribution we shall argue that dissipation is a plausible candidate for such a differential barotropic–baroclinic response. We shall demonstrate that a simple linear model with this mechanism is able to account for several important aspects of the observations in the North Pacific. In particular, the change in the meridional location of the gyre with depth and also its varying longitudinal character may be qualitatively accounted for by a relatively simple model.

The paper is organized as follows: Section 2 develops the simple linear model and analyses a variety of limiting solutions. Section 3 computes horizontal solutions for a variety of idealized forcings as well as an estimate for the actual North Pacific forcing. In section 4, the three-dimensional solutions are then compared with the observations and conclusions drawn as to the implied dissipation rates for the baroclinic modes. Section 5 contains a summary and conclusions.

2. Relevant equations and simple analytical solutions

Consider the usual primitive equations (Gill 1982, pp. 84–85) and make the assumptions of (i) incompressibility, (ii) a Boussinesq approximation, (iii) a hydrostatic approximation, and (iv) an equatorial beta plane. The resulting equations are

$$\frac{du}{dt} - fv = -\frac{1}{\rho_0}\frac{\partial p}{\partial x} + M(u)$$

$$\frac{dv}{dt} + fu = -\frac{1}{\rho_0}\frac{\partial p}{\partial y} + M(v) \qquad \frac{\partial w}{\partial z} + \frac{\partial u}{\partial x} + \frac{\partial v}{\partial y} = 0$$

$$\frac{\partial p}{\partial z} = -\rho g \qquad \frac{d\rho}{dt} = N(\rho),$$

where the symbols M and N denote mixing operators for momentum and density respectively and $f = \beta y$. Consider now a linearization of these equations about a state of rest and a mean vertical density profile:

$$u_t - fv = -\frac{1}{\rho_0}p_x + M(u)$$

$$v_t + fu = -\frac{1}{\rho_0}p_y + M(v) \qquad w_z + u_x + v_y = 0$$

$$p_z = -\rho g \qquad \rho_t + w\overline{\rho}_z = N(\rho).$$

We are motivated to consider such a linear approximation by its great success in the past in explaining very important aspects of the tropical atmosphere and ocean circulations (e.g., Gill 1980; McCreary 1981). Obviously to get more accurate depictions of the subtropical flow we shall require consideration of the effects of nonlinearity and varying mean circulations; however, since our purpose here is only to propose how certain qualitative features of the circulation may be explained, a linear model with constant stratification will suffice. What is the validity of such an approximation for the total flow? As we are interested in large-scale subtropical flows, the Rossby number will be very small, which justifies the neglect the momentum advection terms in the first two equations. The neglect of perturbation advection of perturbation density is less justifiable; however, in most of our domain of interest

it will be small relative to the term $w'\overline{\rho}_z$ (see appendix) and solutions discussed below should not be qualitatively affected on the large scale by its inclusion. As a further simplification we shall, for the present, neglect ventilation processes in the near-surface layers. Such processes evidently play a significant role in determining density structures in such layers and a very simple parameterization of their effects will be considered in the next section.

With this set of approximations, it is well known that a separation of variables in the vertical and horizontal is possible providing we make certain assumptions about the form of the M and N operators (see, e.g., McCreary 1981). For our present purposes we choose the simplest possible form for them, namely that of linear drag; however, more general forms shall be discussed below. The separation of variables means that the vertical parts of each variable satisfies a Sturm–Liouville system. This has a set of eigenfunction solutions each of which specifies the vertical structure of each variable for the so-called vertical modes (i.e., the barotropic and baroclinic modes; see Gill 1982, p. 161). The horizontal parts of each of these modes satisfy shallow-water equations with a shallow water speed derived from the mode's eigenvalue. Imposing the relevant upper boundary condition for surface wind stress in the momentum equations and dropping time dependency (we are interested only in steady flows) allows us to write the horizontal equation for each mode as

$$\begin{aligned} \epsilon u_n - f v_n &= -(p_n)_x + \tau^x/(\rho_0 H_n) \\ \epsilon v_n + f u_n &= -(p_n)_y + \tau^y/(\rho_0 H_n) \\ \epsilon p_n + c_n^2 \nabla \cdot \mathbf{u}_n &= 0, \end{aligned} \tag{1}$$

where the subscript n specifies the vertical mode under consideration, $\boldsymbol{\tau}$ is the surface wind stress, c_n is the shallow water speed of the mode, ϵ is the linear drag coefficient assumed, and H_n is the projection coefficient of the windstress onto the mode n and is determined from the upper boundary condition. The reader is referred to Cane and Sarachik (1977) for further discussion of these equations and the precise meaning of the variables. For the rest of this section we drop the subscripting of each vertical mode for pedagogical convenience. The equations may be reduced to one equation in v (see Gill 1982, p. 467):

$$\frac{\epsilon^3}{c^2} v + \frac{\epsilon f^2}{c^2} v - \epsilon v_{xx} - \epsilon v_{yy} - \beta v_x = \text{forcing}.$$

If we assume that ϵ is small, we can neglect the first term on the left-hand side. Further, if we assume that the forcing has a characteristic zonal wavenumber k and that $\epsilon k \ll \beta$, then the third term is much smaller than the last and we can neglect it. We shall be interested in zonal scales of $\approx 3.0 \times 10^6$ m, so this assumption is equivalent to $\epsilon \ll 10^{-5}$ s^{-1}, which will be met by our solutions.[3] The neglect of these two terms is equivalent to dropping the term ϵv in the second equation of (1), an assumption known as the long-wave approximation (see Cane and Sarachik 1977). We now nondimensionalize variables by dividing velocities by c and horizontal distance by the equatorial Rossby radius ($\sqrt{c/(2\beta)}$). This implies that p and $\boldsymbol{\tau}/\rho_0 \equiv \mathbf{X}$ (the pseudostress) are divided by c^2 whereas ϵ is multiplied by $\sqrt{1/(2\beta c)}$. The relevant equations for these new nondimensionalized variables are

$$\epsilon u - \frac{1}{2} y v = -p_x + X^x/H \qquad \frac{1}{2} y u = -p_y + X^y/H$$

$$\epsilon p + \nabla \cdot \mathbf{u} = 0.$$

This flow is formally separable into a part that is the traditional Ekman flow and a remainder that represents wave effects:

$$\mathbf{u} = \mathbf{u}_E + \mathbf{u}_p,$$

where

$$-\frac{1}{2} y v_E = X^x/H \qquad \frac{1}{2} y u_E = X^y/H,$$

so therefore

$$\epsilon u_p - \frac{1}{2} y v_p = -p_x \tag{2}$$

$$\frac{1}{2} y u_p = -p_y \tag{3}$$

$$\begin{aligned} \epsilon p + \nabla \cdot \mathbf{u}_p = -\nabla \cdot \mathbf{u}_E &= \frac{2}{H}\left[\frac{\partial}{\partial y}\left(\frac{X^x}{y}\right) - \frac{\partial}{\partial x}\left(\frac{X^y}{y}\right)\right] \\ &= \frac{1}{H} w_E \equiv F_E, \end{aligned} \tag{4}$$

where w_E is the Ekman pumping velocity. This kind of separation of the flow has been used previously by Phlips (1987) to look at the equatorial region. Here we use it to examine the subtropics. It is interesting to note that these equations are identical in form to those used by Gill (1980) to model the response of the tropical atmosphere to diabatic heating. Here the forcing represents Ekman pumping rather than diabatic heating. It is also interesting to note that very similar equations have been used by Kawase (1987) and Cane (1989) to model the abyssal circulation.

We now introduce the ancillary variables $q = p + u_p$, $r = p - u_p$ and obtain from Eq. (2) plus Eq. (4), and Eq. (2) minus Eq. (4) together with Eq. (3):

[3] We shall retain the fourth term as for our solutions, variations in the meridional direction are more rapid than those in the zonal direction implying that this term is generally significantly larger than the third.

$$\epsilon q + q_x = \left(\frac{1}{2}y - \partial_y\right)v + F_E$$

$$\epsilon r - r_x = -\left(\frac{1}{2}y + \partial_y\right)v + F_E$$

$$\left(\partial_y + \frac{1}{2}y\right)q + \left(\partial_y - \frac{1}{2}y\right)r = 0. \tag{5}$$

Note that we are dropping the p subscript.

These equations can now be expanded again into meridional modes with the useful expansion basis being parabolic cylinder functions. In order to facilitate this analysis at higher latitudes, we use parabolic cylinder functions with a different normalization to the usual $D_m(y)$:

$$E_m = [(m-1)(m-3)(m-5)\cdots 1]^{-1} D_m.$$

The advantage of this normalization is that the E_m are approximately equal in amplitude whereas the D_m increase rapidly with m. This modified normalization improves convergence outside the equatorial region of quantities that are a sum of the parabolic cylinder functions. Using the lowering and raising relations for D_m (see Gill 1982, p. 439) we obtain analogous relations for E_m:

$$\begin{pmatrix} \left(\partial_y + \frac{1}{2}y\right)E_m \\ \left(\partial_y - \frac{1}{2}y\right)E_m \end{pmatrix} = \frac{m(m-2)\cdots 1}{(m-1)(m-3)\cdots 1}\begin{pmatrix} E_{m-1} \\ -E_{m+1} \end{pmatrix}$$

$$\equiv \gamma(m)\begin{pmatrix} E_{m-1} \\ -E_{m+1} \end{pmatrix}. \tag{6}$$

Expanding q, r, and v in terms of these renormalized functions we obtain from Eqs. (5) and (6),

$$(\partial_x + \epsilon)q_m = \gamma(m-1)v_{m-1} + F_m \tag{7}$$

$$(\epsilon - \partial_x)r_m = -\gamma(m+1)v_{m+1} + F_m \tag{8}$$

$$r_m = \frac{m+2}{m+1}q_{m+2}, \tag{9}$$

where F_m is the projection of the Ekman forcing F_E onto the mth parabolic cylinder function. Substituting Eq. (9) in Eq. (8) and lowering indices by 2 we obtain

$$(\epsilon - \partial_x)mq_m = (m-1)\gamma(m-1)v_{m-1} + (m-1)F_{m-2}.$$

Combining this with Eq. (7) we obtain

$$[\epsilon(2m-1) - \partial_x]q_m = (m-1)[F_m + F_{m-2}] \tag{10}$$

which is the equation we will solve.

Consider now an idealized Ekman pumping, which for simplicity is constant in the region $0 \le x \le L$ but for now has arbitrary meridional dependency. The particular solution for such forcing from Eq. (10) is given by

$$q_m^s = \frac{(m-1)[F_m + F_{m-2}]}{\epsilon(2m-1)} \equiv \frac{A_m}{\epsilon}. \tag{11}$$

Further, we shall assume that the Kelvin mode ($m = 0$) plays an insignificant role in the solution as we are in the subtropics.[4] It follows easily then that the general solution to Eq. (10) is

$$q_m(x) = \frac{A_m}{\epsilon}[1 - \exp((2m-1)\epsilon(x-L))]. \tag{12}$$

We are using here the assumed insignificance of the equatorial Kelvin mode to impose $q_0(L) = 0$. The vanishing of $u_m = (q_m - r_m)/2$ at the eastern boundary then implies [using Eq. (9)] that $q_m(L) = 0$ for all m. This boundary condition then allows us to derive our solution.

The solution for pressure is

$$p_m(x) = \frac{1}{2}(q_m + r_m) = \frac{1}{2}\left(q_m + \frac{m+2}{m+1}q_{m+2}\right) \tag{13}$$

$$= \frac{1}{2\epsilon}A_m(1 - \exp[(2m-1)\epsilon(x-L)]) + \frac{m+2}{m+1}\frac{A_{m+2}}{2\epsilon}(1 - \exp[(2m+3)\epsilon(x-L)]). \tag{14}$$

We consider now some special limits. First consider the case for which $2m\epsilon(x-L)$ is small. In this case we can replace the exponentials in Eq. (14) with unity plus the exponent. Using Eq. (11) the above equation reduces to

$$p_m = (x-L)[(m-1)F_{m-2} + (2m+1)F_m + (m+2)F_{m+2}],$$

and then using the relations (6) it follows easily that

$$p(x, y) = \frac{y^2}{4}F_E(x-L). \tag{15}$$

This is simply the Sverdrup relationship (see Gill 1982, p. 465), which holds for an inviscid flow; it is the solution to Eqs. (2)–(4) with $\epsilon = 0$.

Next consider the case for which $2m\epsilon(x-L)$ is large and negative. This will occur for the large damping case or when x is small relative to L (i.e., in the western part of the basin). In this case the exponential terms in Eq. (14) are small compared to unity and the p_m are approximately independent of x. The solution then is proportional to the zonally independent case, which we can

[4] This approximation is less justified for the barotropic mode but the essentially inviscid nature of this mode shall allow this issue to be bypassed. See below.

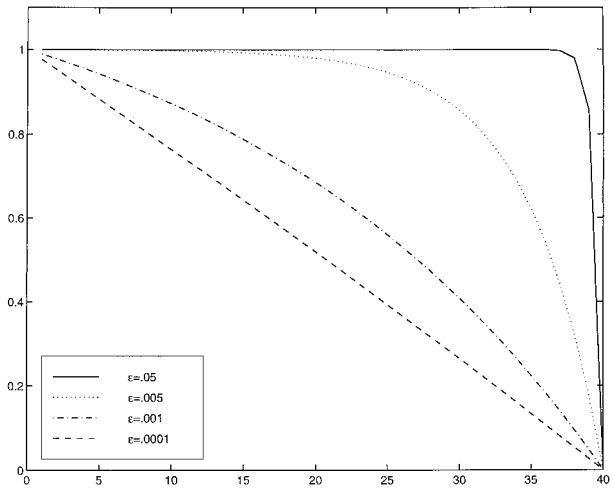

FIG. 2. Plots of the q_m (x) function for varying choices of the dissipation parameter ϵ (see text). The dashed line has $\epsilon = 0.0001$; the dash–dot line has $\epsilon = 0.001$; the dotted line has $\epsilon = 0.005$ while the solid line has $\epsilon = 0.05$.

obtain directly from the original Eqs. (2)–(4) by dropping terms with x derivatives. These then reduce to

$$v_{yy} - \frac{1}{4}y^2 v = (F_E)_y \tag{16}$$

$$p_y = -\frac{1}{4}y^2 v/\epsilon. \tag{17}$$

For the case which shall interest us, y is large ($\sim$10) and the forcing varies reasonably slowly compared to the Rossby radius. In such a case the first term in Eq. (16) may be neglected and we obtain simply

$$p \sim F_E/\epsilon. \tag{18}$$

By numerically integrating Eqs. (16) and (17) with Gaussian forcings of varying half-widths we have confirmed that Eq. (18) is indeed a good approximation, even when the half-width is a fraction of the Rossby radius. The proviso here is that y must be large. When it is not, the approximation (18) breaks down and the solution takes on the character discussed by Gill (1982, p. 467); that is, it shows a greater amplitude equatorward of the symmetric Gaussian forcing used.

The two solutions (15) and (18) obviously imply different meridional locations for the pressure response to Ekman pumping. In the case of the pumping associated with the variation from trade easterlies to midlatitude westerlies it implies that the Sverdrup solution (15) will be located more poleward. In the next section we shall show that the difference in gyre location can amount to more than 10° in latitude, a difference that seems to also occur in the observations.

We now consider the transition between the two limiting solutions. Displayed in Fig. 2 is a plot of $q_m(x)$ for values of ϵ varying between the two solutions. Solutions have been scaled to have the same value at the western boundary. The heavy dashed line solution is the Sverdrup one, while the light solid line solution is close to the zonally invariant one for values of x not too close to L. Clearly intermediate solutions tend to resemble more the Sverdrup relation in the east where $|m\epsilon(x - L)| \ll 1$ and more the zonally invariant Ekman pumping response in the west where $|m\epsilon(x - L)| \gg 1$. Given the discussion of the differences meridionally between the two, one should expect intermediate solutions for the subtropical gyre to slant from the southwest to the northeast.

3. Horizontal solutions for various forcings

We consider solutions first for an idealized zonally invariant patch of forcing. The forcing chosen is intended to resemble the observed transition between tropical easterlies and midlatitude westerlies and has the form

$$w_E = \begin{cases} 1, & y_T < y < y_M \\ (y - y_T + \Delta y)/\Delta y, & y_T - \Delta y < y < y_T \\ (y_M - y + \Delta y)/\Delta y, & y_M < y < y_M + \Delta y \\ 0, & \text{otherwise.} \end{cases}$$

As in the previous section we assume that this holds for the zonal domain $0 < x < L$ and the Ekman pumping is zero outside. The dimensionless parameter choices are

$$(y_T, y_M, \Delta y, L) = (7.5, 15.0, 2.5, 20).$$

For the first baroclinic mode ($c \sim 3$ m s^{-1}) these choices can be multiplied by about two degrees to obtain approximate latitudinal and longitudinal bounds. The forcing together with the corresponding zonal wind stress are depicted[5] in Fig. 3. We consider now $\epsilon = 0.025$, 0.001, 0.0001, which for the first baroclinic mode correspond to damping times of approximately 40 days, 2.8 yr, and 28 yr respectively.

Plots of pressure–dynamic height are displayed in Figs. 4a–c. The transition between the two limiting solutions discussed in the previous section is quite apparent: The maximum of dynamic height shifts from a broad peak centered on the western boundary at $y = 11.25$ for high dissipation to a more peaked maximum centered at $y = 15$ for low dissipation. Other features include a greater zonal gradient in the east, as predicted in the previous section, and a more zonally uniform solution at higher latitudes. This latter property is due to the fact that Rossby modes propagate at increasingly slower speeds at higher latitudes and consequently the high dissipation solution becomes more relevant here. Mathematically one can see this dependency in Eq. (14)

[5] We use the first 200 meridional components to compute this solution. This is sufficient for reasonable solution convergence.

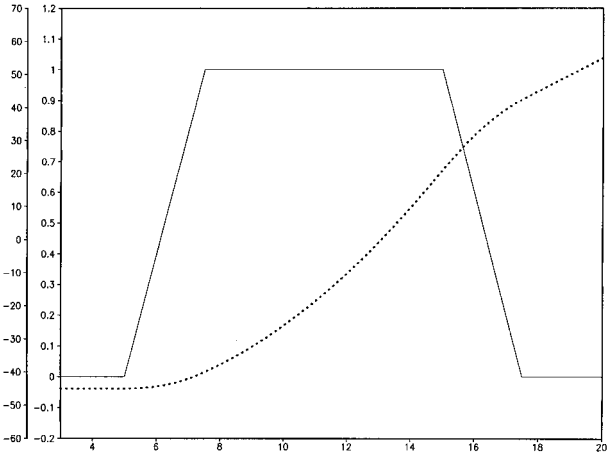

FIG. 3. The idealized Ekman forcing (solid line) and corresponding wind pseudostress (dotted line) used to construct analytical solutions. The extreme left vertical axis is for the pseudostress while the inner axis is for the Ekman pumping (see text).

through the factors $2m - 1$ and $2m + 3$ in the exponents. It is interesting to compare these solutions mathematically with similar ones of Kawase (1987) for the abyssal circulation.

We now consider the observed forcing. First the annually averaged Hellerman and Rosenstein (1983) wind stress data was used to construct two relevant fields—the Ekman pumping velocity (under the assumption of a β plane) and f^2 times this field, which represents the meridional component of the Sverdrup solution for p, namely, Eq. (15). A horizontal plot of the first field (not shown) shows it to be reasonably zonally uniform, so displayed in Fig. 5 are zonally averaged versions of the two fields (the zonal averages are from 150°E to 135°W where zonal uniformity is a reasonable approximation). It is apparent that the Ekman pumping peaks well to the south (~15°N) of where the Sverdrup solution does (~30°N). This situation therefore resembles the idealized case considered above. Making the assumption that the forcing is zonally uniform and using the pumping cross section shown in Fig. 5, we obtain solutions corresponding to Figs. 3a–c with the scaling set by a shallow water speed of 3.2 m s^{-1}. These are displayed in Figs. 6a–c and show a peak in pressure at just less than 20°N for the high dissipation case: a reasonably broad peak between 20°N and 30°N for the moderate dissipation case and a strong pressure peak at 30°N in the case of weak dissipation. Other features of the idealized case are apparent: In particular the weaker the dissipation the greater the zonal gradient of pressure, which corresponds with the transition from the zonally invariant case to the Sverdrup solution.

4. Observed structure of the gyre and vertical solutions

Finally we turn to direct observations of the subtropical gyre. We use the recently updated annually averaged Levitus and Boyer (1994) density fields for the North Pacific. We chose to use density observations directly rather than to calculate pressure–dynamic height because the latter quantity requires an arbitrary reference level for calculation and also the former quantity shows meridional shifts more clearly. The two quantities are of course simply related by the hydrostatic relation and hence each baroclinic mode should have the same horizontal structure in both quantities. What is interesting about the observations is the variation with depth of the gyre. Displayed in Figs. 7a–c is the density

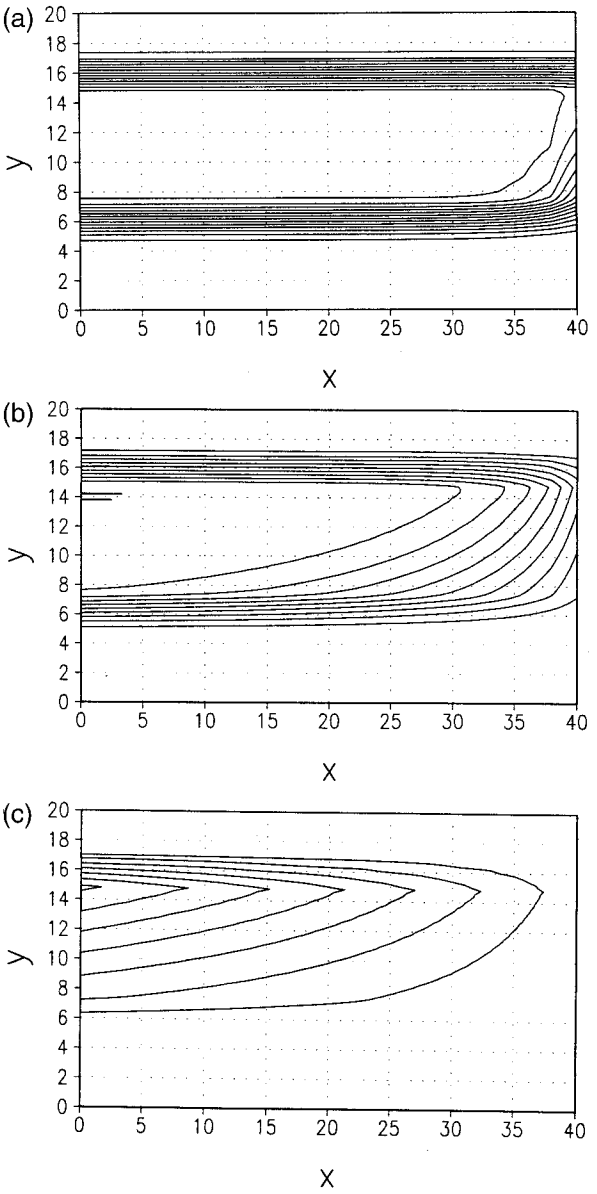

FIG. 4. (a) The solution for pressure for the idealized forcing and high dissipation ($\epsilon = 0.025$). Contour interval is 0.1 (b) Same as (a) but for moderate dissipation ($\epsilon = 0.001$). Contour interval is 1.0. (c) Same as (a) but for low dissipation ($\epsilon = 0.0001$). Contour interval is 10. Note that contours have been rescaled for comparison purposes.

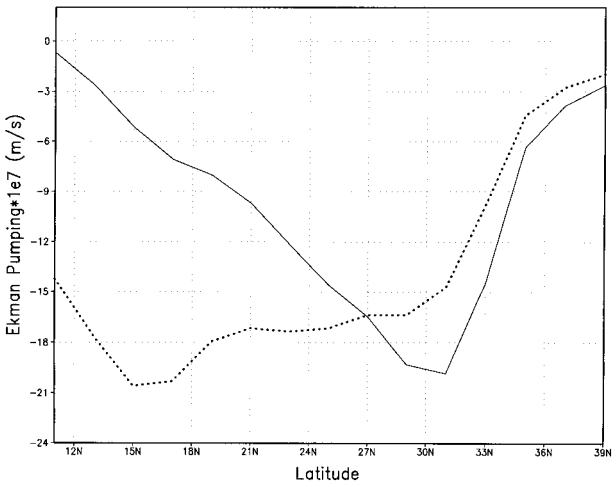

FIG. 5. Zonal-average Ekman pumping velocity for the North Pacific together with the meridional part of the Sverdrup solution to this forcing.

field at 110 m, 250 m, and 500 m. These show a clear migration of the gyre from around 15°N at shallow levels to around 30°N in the deep. Also apparent is a change from a more zonally uniform nature at shallow levels to a gyre that varies linearly in the zonal direction at depth. In terms of the solutions discussed in the previous section, it seems that the higher dissipation solutions apply at shallow levels while the low dissipation cases are more relevant at depth.

As discussed in section 2 above it may be expected that surface ventilation processes will play some role in setting densities at the 110-m level. Such processes involve strong vertical mixing during late winter and early spring (see Pedlosky 1996). There is a transfer of the cold surface waters to depth via very deep mixed layers. This is well known to be a difficult process to model well, and we shall consequently adopt a very simple parameterization of its effect just to allow a better comparison of our solutions with the observations: The mixed layer at the latitudes under consideration reaches its maximum depth in late winter, so we shall assume that water at 110 m (our comparison point with the observations) is modified by turbulent contact with the surface at that time. We thus assume that the ventilation acts to add a density perturbation to our solutions that is equal to the observed late winter meridional surface density profile north of a critical latitude. This latitude is determined by whether, at some point in the annual cycle, the water at 110 m is in turbulent contact with the surface *even if such contact is intermittent.* A reasonable choice for such a latitude is around 20°N as this is the approximate limit to which synoptic incursions from the midlatitudes are able to penetrate into the subtropics during winter. Such incursions in the North Pacific are associated often with very cold surface air and hence the possibility of deep oceanic mixed layers. The mean mixed layer depth in late winter in the North Pacific exceeds 100 m north of around 25°–30°N (see Pedlosky 1996, p. 234), however one should expect that intermittent mixed layers of this depth should be observed farther equatorward.

The greater applicability of damped solutions at shallow levels and less damped solutions at depth can be explained by consideration of the character of vertical modes[6] (see McCreary 1981; Philander 1990): The higher modes with significant projection from wind stress tend to have relatively more of their amplitude near the surface compared with lower modes, which are more uniform in amplitude with depth. This is illustrated in Figs. 8a,b, which shows the density perturbations with depth of the significantly forced vertical modes. The modes were calculated using a background stratification appropriate to the North Pacific subtropics (25°N at the date line), which was obtained from the 33 levels of Levitus and Boyer observations. This result implies that the behavior of the density gyre closer to the surface will be more heavily influenced by the higher order baroclinic modes *provided* they have significant projection from the surface wind stress. This is an issue because such projection tends to be different in the subtropics compared to the equatorial region, which is perhaps more familiar to some readers. The amplitude of this projection is given by the value of the normalized pressure vertical eigenvector at the surface. This is plotted in Fig. 8c together with the corresponding shallow water speed. As can be seen there is significant projection throughout the vertical spectrum.[7] Note that this situation is different from the equator where Cane (1984) showed that there is a greater relative projection onto the lower-order modes.

We note next that for a fixed dissipation rate, the solutions derived from Eq. (14) for the higher order baroclinic modes tend toward the more highly damped case. This follows because the exponents in Eq. (14) when redimensionalized are proportional to $m\epsilon(x - L)/c$, where c is the shallow water speed. Clearly c drops as the baroclinic mode order increases. In addition, because the Rossby radius also drops, the Ekman forcing F_E will project more heavily onto horizontal modes with larger values of m (in nondimensional units the forcing

[6] Recall that such modes are eigenvectors of the Sturm–Liouville system, which applies to the vertical structure of our solutions (see Gill 1982, p. 161). They are depth-dependent structure functions for both pressure and momentum. Different structure functions for a particular baroclinic mode apply for other variables such as vertical velocity. We normalize our eigenvectors here by dividing by the vertical integral of the eigenvector squared (the so-called L_2 norm).

[7] Note that at the high end of the spectrum there is likely to be noisiness in the specific projection onto particular modes due to small amounts of vertical scale noise in the observed vertical stratification profile. The ragged values here are evidence of this. Nevertheless there is still significant real projection onto modes greater than 10. It is to be noted, however, that for the very high modes (20–30) the effects of dissipation in our model become very important and so they contribute only in a minor way to the total solution.

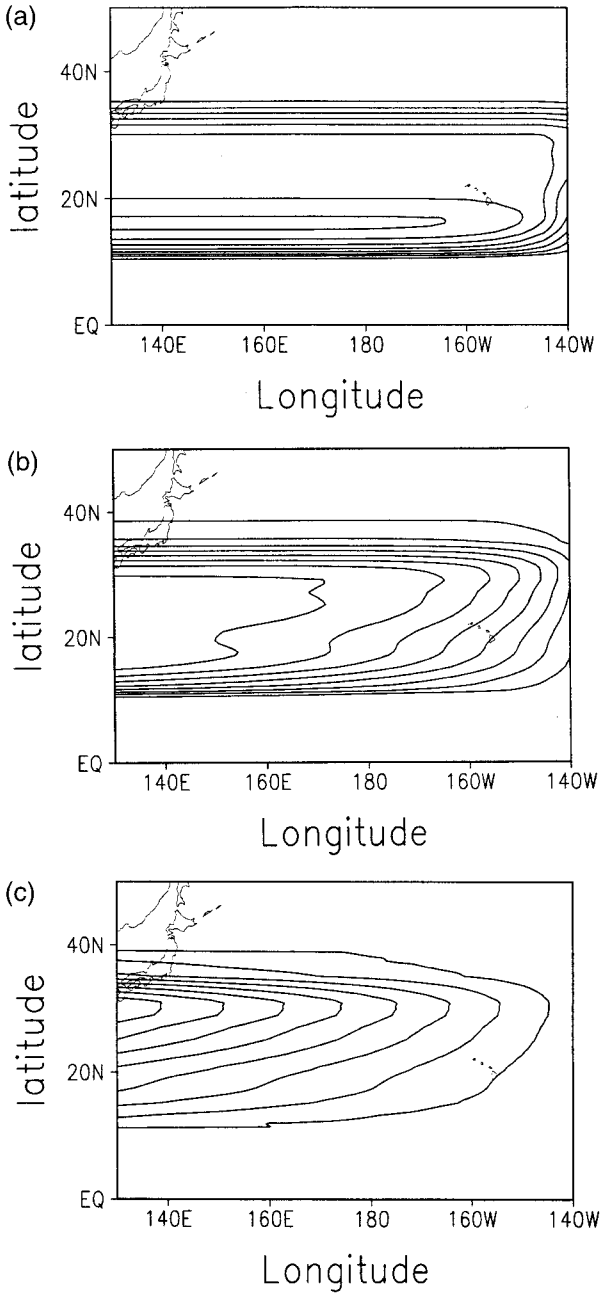

FIG. 6. As in Figs. 4a–c but for the case of a representation of observed Ekman forcing.

occurs at a greater distance from the equator). Both of these factors ensure that the higher-order modal gyre solutions will more resemble the zonally invariant solution discussed in the previous section.

A final point worth noting is that at significant depth (say 500 m) the eigenvector for density appears to have equal amplitude for the first few modes, so one might not expect at first glance that the lowest-order modes should dominate the solution at this level. In fact this *does* occur because the dimensionalized F_E involved in the solution (14) is proportional to c^2.

In order to confirm that the three factors discussed above combine to produce solutions resembling the observations, we use the three-dimensional linear model discussed in section 2. With regard to dissipation we first use a constant value for all modes, which is intended to represent horizontal mixing processes. Vertical mixing is often thought to be highly mode dependent (see McCreary 1981) because of the increasing vertical structure with mode number and will be considered below. Forcing is taken from the observations in the same manner as at the end of the previous section. In addition, to model the influence of surface mixed layer processes (see the discussion above) a linearly increasing density offset was added to this solution northward of 20°N at the depth of 110 m (no offset is added at deeper levels). All further solutions below have this offset added. Its value was determined by calculating the approximate surface poleward gradient of density from the Levitus and Boyer (1994) climatology for the month of March (taken to represent late winter) in the mid North Pacific and is set at 0.001 56 g cm^{-3} per 10° of latitude.

Solutions proportional to density perturbations at depths 110 m, 250 m, and 500 m are displayed in Figs. 9a–c and show the character already noted in the observations. We have used here a damping time of 3 years for all modes. Solutions for a damping time of 1 year (not shown) were very similar to those for 3 years. Those for a damping time of 15 years (Figs. 9d–f) were somewhat different. Overall the more highly damped solutions are in better agreement with the observations particularly at 110 and 250 m. Note the larger contour intervals for Figs. 9d–f. This result therefore appears to provide some constraint on the value of subtropical oceanic isopycnic dissipation. If we assume that such damping has the form of a Laplacian and acts on structures of the scale depicted in Fig. 9 (i.e., around 1000 km), then a value of around 1000 $m^2\ s^{-1}$ is indicated for the viscosity and diffusivity—a value commonly assumed in good non-eddy-resolving ocean models to simulate this subgrid scale mixing.

As already mentioned we might expect vertical mixing processes to act in a highly modal-dependent fashion with dissipation increasing strongly with mode number. Here we examine this question using the vertical mixing parameterization of McCreary (1981):

$$\nu,\ \kappa \sim \frac{1}{N^2}, \tag{19}$$

where ν and κ are the coefficients of vertical viscosity and diffusivity respectively while N is the Brunt–Väisälä frequency. Equation (19) implies that the modal dissipation varies as

$$\epsilon_n = A/c_n^2 = \epsilon_1 c_1^2/c_n^2, \tag{20}$$

where c_n is the shallow water speed relevant to the nth mode. Solutions were calculated with *only* this kind of

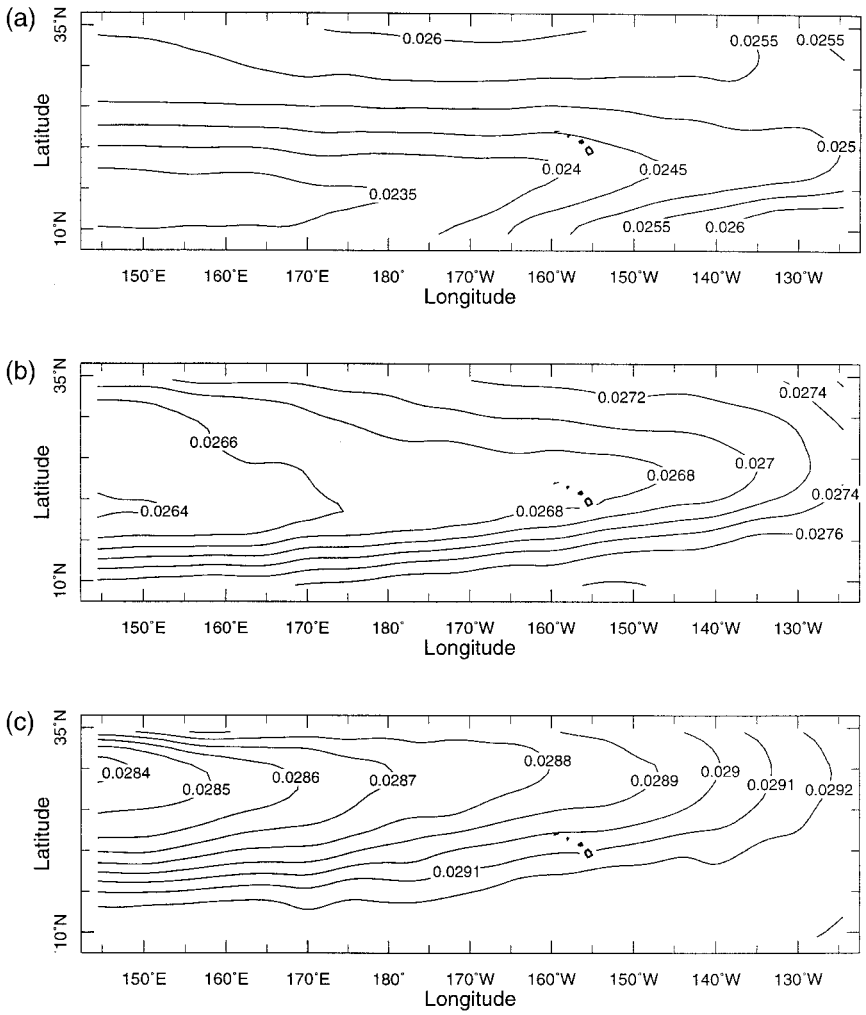

FIG. 7. (a) The annually averaged Levitus and Boyer (1994) density field at depth 110 m. Units are g cm^{-3} − 1. Contour interval is 0.0005. (b) The same as (a) but for depth 250 m. Contour interval is 0.0002. (c) The same as (a) but for depth 500 m. Contour interval is 0.0001.

dissipation and with small and large values for ϵ_1^{-1} (3 and 60 years, respectively). Agreement with observations (not shown) is not as good as in Figs. 9a–c, which argues for the importance of horizontal mixing. Of course some vertical (diapycnal) mixing is present in the real ocean and, if we add the vertical dissipation with the large value for ϵ_1^{-1} to the constant value assumed for horizontal mixing in Figs. 8a–c, we again obtain a reasonable solution (Figs. 10a–c). Such a vertical dissipation rate corresponds to a value of 10^{-3} m^2 s^{-1} for $N^2 = 5 \times 10^{-6}$ s^{-2}. The latter value is not unreasonable for the mixed layer, while the former is not atypical of values often used in the mixed layer of high-resolution ocean models. It is interesting to note that these results suggest that for low-order baroclinic modes, horizontal rather than vertical mixing may be the major dissipation mechanism and that a decay time of several years is indicated.

Finally it is worth commenting on the barotropic mode. Here, because the shallow water speed is so fast (~200 m s^{-1}), dissipation at the rates discussed above is essentially irrelevant and the steady solution is thus very close to the inviscid Sverdrup solution given in Eq. (15). The classical conclusions of Sverdrup theory for depth-averaged flow (primarily the barotropic flow) are therefore not affected by the discussion in this paper.

5. Summary and discussion

The influence of dissipation on the steady state wind-forced shallow-water equations (β plane) in the subtropics has been explored by using a convenient flow separation and a well-known solution technique. It is found that solutions for pressure vary between a zonally uniform structure proportional to the Ekman pumping when dissipation is high through to a solution varying linearly with longitude and displaced poleward of the Ekman pumping when the dissipation is small. The latter

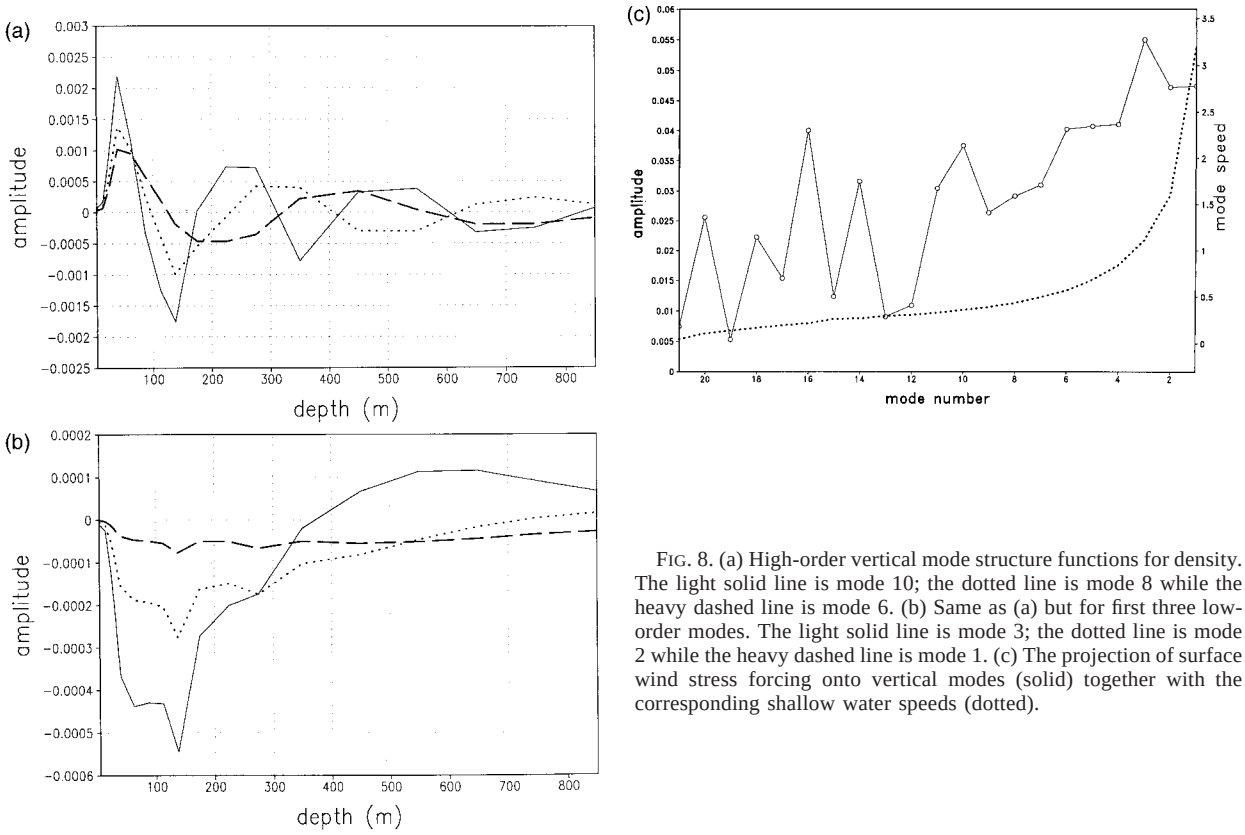

FIG. 8. (a) High-order vertical mode structure functions for density. The light solid line is mode 10; the dotted line is mode 8 while the heavy dashed line is mode 6. (b) Same as (a) but for first three low-order modes. The light solid line is mode 3; the dotted line is mode 2 while the heavy dashed line is mode 1. (c) The projection of surface wind stress forcing onto vertical modes (solid) together with the corresponding shallow water speeds (dotted).

solution is the classical one due to Sverdrup (1947). In the subtropical North Pacific the meridional displacement between the two solutions amounts to about 15°.

Observations of the North Pacific gyre show that at shallow levels it resembles the highly damped solution, while in the deep it resembles the Sverdrup solution. By extending our two-dimensional solutions in the obvious manner to the usual three-dimensional barotropic/baroclinic modal decomposition, we find that we are able to reproduce these observations to a fair extent with reasonable assumptions about the rate of horizontal and vertical mixing. The shallow-level solutions are dominated by higher order baroclinic modes, which are more effectively damped than the low order modes for a given constant dissipation. Conversely deep solutions are dominated by the first few baroclinic modes, which are much less damped. It is concluded that these latter modes are likely to be more dissipated by horizontal rather than vertical mixing[8] and that the timescale of this process is estimated to be of the order of several years. Such a decay time is commonly assumed in intermediate coupled models of the equatorial Pacific (e.g., Zebiak and Cane 1987) and the implied value for Laplacian viscosity and diffusivity (10^3 m^2 s^{-1}) is widely used in good non-eddy-resolving ocean models. Given this situation, it would be interesting in a further study to examine the dependence of the solutions here on various forms of horizontal mixing. Such parameterizations are, of course, an important area of uncertainty in ocean modeling.

The current study focussed on the Northern Pacific subtropical region. It would be very interesting to extend the comparison here between theory and observations to other subtropical and indeed subarctic regions. The latter regions would require some minor modification of the β-plane model, which has less validity at higher latitudes.

A further study, which is being planned, will examine the sensitivity of our solutions to background states of barotropic and low-order baroclinic currents. Such a study would help address the relative importance of the mechanisms proposed here and those previously proposed by Rhines and Young (1982a).

An issue addressed in theories such as Rhines and Young (1982a) is that of potential vorticity (PV) homogenization: Observations show that the middle thermocline of the subtropics has reasonably constant values for this field (see, e.g., Keffer 1985). Rhines and Young explain this process as follows: In their inviscid nonlinear, nonventillated model, PV is conserved. The addition of interlayer linear drag has the effect of adding a diffusive

[8] Another possibility is that real vertical mixing processes are less mode dependent in their dissipative effects than that assumed in the model of McCreary (1981).

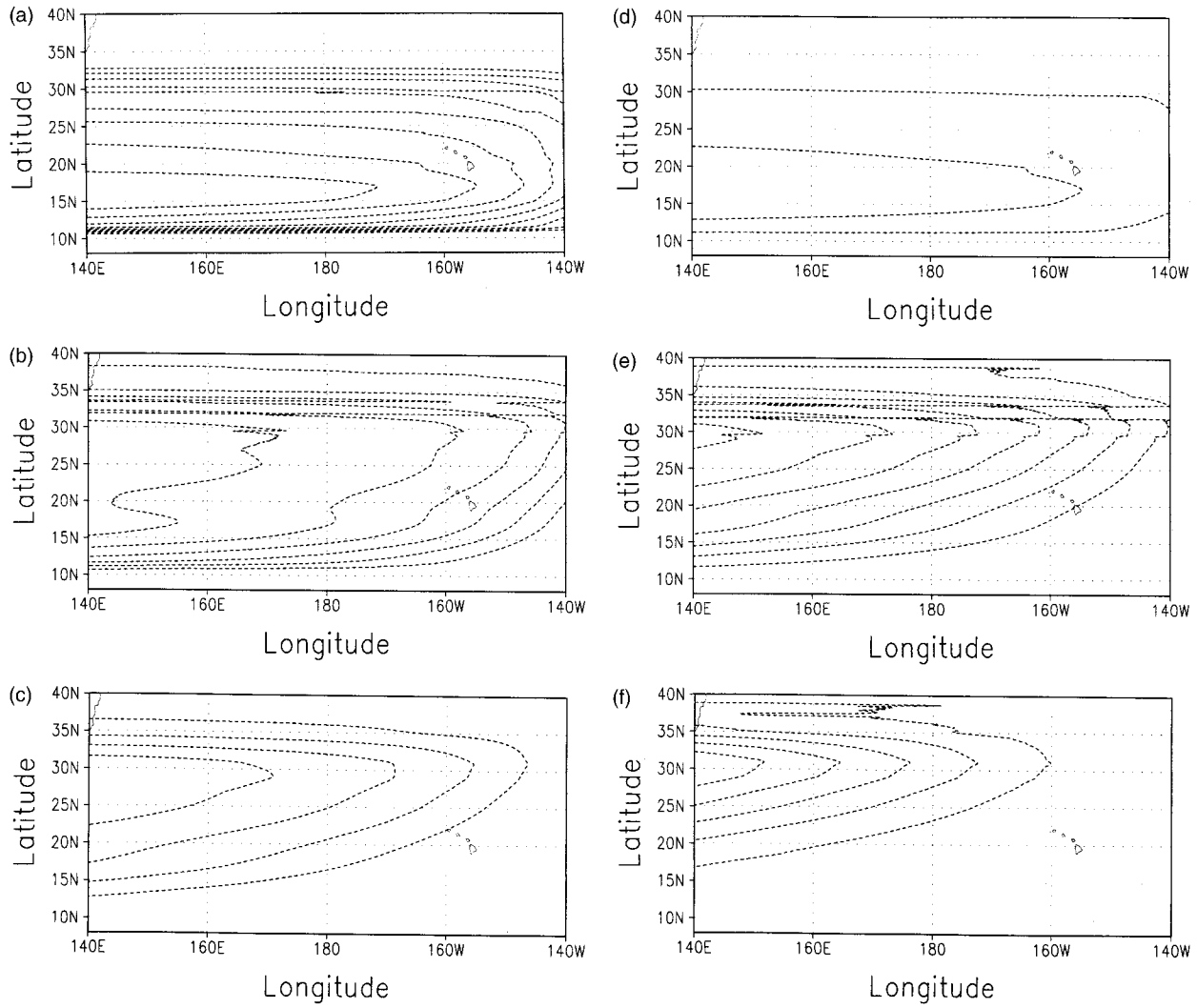

FIG. 9. The modeled quantities corresponding to the observations in Fig. 7 for a variety of constant dissipations: (a)–(c) The case $\epsilon = (3\ \text{yr})^{-1}$. (d)–(f) The case $\epsilon = (25\ \text{yr})^{-1}$. The contour intervals are the same as Figs. 7 for a–c. The contour interval in (d) is 0.002; 0.0008 for (e); and 0.0002 for (f).

sink in the PV equation. Advection of PV around the subtropical gyre ensures that this quantity is approximately constant on closed streamlines *providing* that the diffusion of PV is not too strong (equivalently that the interlayer linear drag is small). Once the boundary of the closed streamline has established an approximately constant PV, this value is slowly diffused into the interior of the loop, eventually establishing a pool of homogenized PV.

Clearly for this process to take place, advection of PV is required and this is not present in the linear model considered in this paper. Consistent with this, the model PV near the mid thermocline (Fig. 11) does not show quite the same degree of PV homogenization as the observations (compare with Keffer's Fig. 11), particularly in the central Pacific. How does this relate to observations of density such as Fig. 1? Pedlosky (1996) shows that to a reasonable approximation,

$$\text{PV} = f\rho_z.$$

Thus if PV were completely homogenized meridionally, the increase in f with latitude would be balanced by a spreading of density contours in the thermocline, as may indeed be noted in Fig. 1. Thus our simple linear model is able to account for the meridional shift in gyre location with depth as well as the concomitant changes in zonal structure but is less able to explain the ''fanning out'' of the thermocline with increasing latitude. Evidently the linear processes discussed in this paper may be partially responsible for the structure observed, but nonlinearity probably needs to be invoked to get full agreement (see also the appendix below). Such a discrepancy is only to be expected given the relative simplicity of the model deployed here, which is used only to illustrate how dissipation can account for a number of characteristics of the observed gyre structure, not all of them.

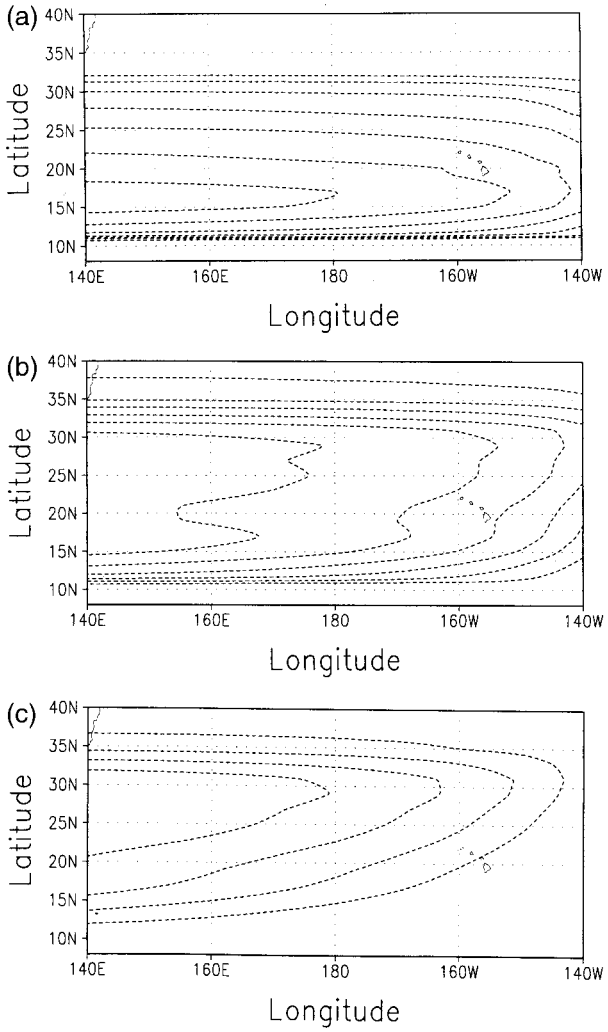

FIG. 10. As in Figs. 9a–c but with a vertical dissipation term added which acts selectively on the vertical modes (see text).

Acknowledgments. The authors wish to thank two anonymous reviewers who helped to significantly improve an earlier version of this paper. The first author wishes to thank the hospitality of the International Research Institute for Climate Prediction at Lamont-Doherty Earth Observatory in New York where most of this work was carried out.

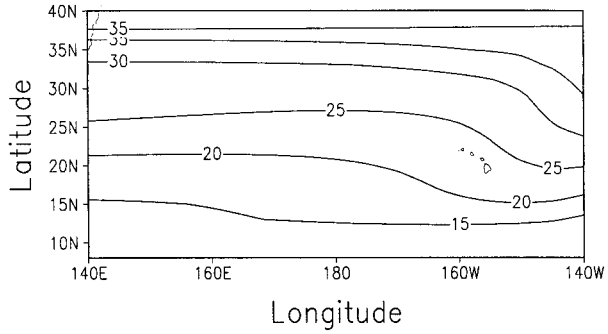

FIG. 11. The midthermocline potential vorticity from the 3D model. Units are the same as those used by Keffer (1985).

APPENDIX

Relative Importance of Nonlinearities

As noted in the text, our interest in large-scale flows means that we can neglect the advection of momentum terms from the primitive equations due to the smallness of the Rossby number. We consider here therefore only the likely effects of the advection of density. This is approximately assessed by calculating the value of these terms for the 3D model configuration displayed in Figs. 9a–c. The value of the linear term retained in our model, namely $w'\overline{\rho}_z$, was also calculated for comparison. Over most of the domain that we have considered the advection terms are small compared with the linear term. In certain reasonably small-scale areas however the terms can become comparable, suggesting that there may be a minor nonlinear correction to the large-scale linear solutions presented in this paper. This may be confirmed by viewing, for example, horizontal plots of the terms at 250 m in Fig. A1. It is evident that advection may play some role in the northeast of the gyre and, in fact, more detailed analysis of the nonlinear terms sug-

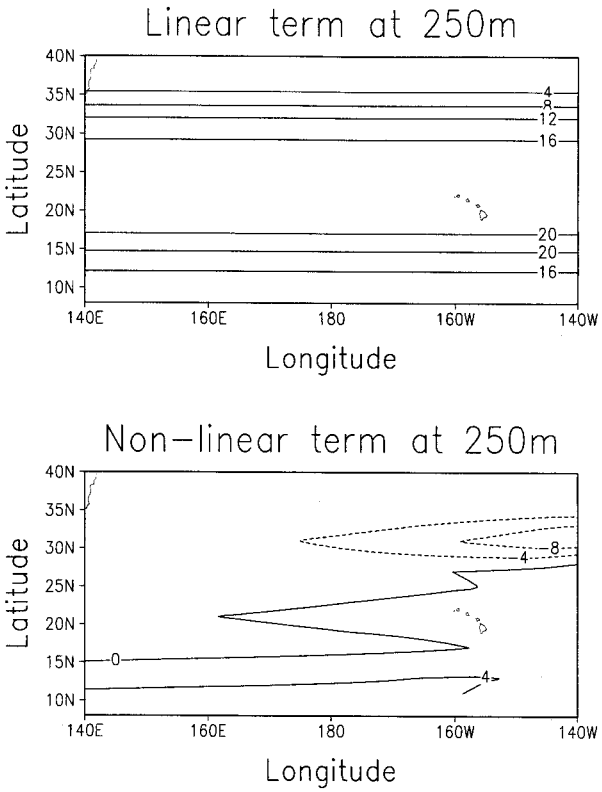

FIG. A1. (a) The values of the linear density tendency term $w'\overline{\rho}_z$. (b) The value of the density advection tendency term. Units for both frames are 10^{-9} kg m^{-3} s^{-1}.

gests that it will act to drag the gyre depression southward here. This effect may indeed be noted in the observations (cf. Figs. 7b and 9b).

REFERENCES

Anderson, D. L. T, and A. E. Gill, 1975: Spin up of a stratified ocean with application to upwelling. *Deep-Sea Res.*, **22,** 583–596.

Cane, M. A., 1989: A mathematical note on Kawase's study of the deep ocean circulation. *J. Phys. Oceanogr.,* **19,** 548–550.

——, and E. S. Sarachik, 1977: Forced baroclinic ocean motions II. The linear equatorial bounded case. *J. Mar. Res.*, **35,** 395–432.

Chelton, D. B., and M. G. Schlax, 1996: Global observations of oceanic Rossby waves. *Science,* **272,** 234–238.

Cipollini, P., D. Cromwell, M. S. Jones, G. D. Quartly, and P. G. Challenor, 1997: Concurrent altimeter and infrared observations of Rossby wave propagation near 34°N in the northeast Atlantic. *Geophys. Res. Lett.,* **24,** 889–892.

Dewar, W. K., 1998: On ''too-fast'' baroclinic planetary waves in the general circulation. *J. Phys. Oceanogr.*, **28,** 1739–1758.

Gill, A. E., 1980: Some simple solutions for heat induced tropical circulation. *Quart. J. Roy. Meteor. Soc.*, **106,** 447–462.

——, 1982: *Atmosphere–Ocean Dynamics.* Academic Press, 662 pp.

Hellerman, S., and M. Rosenstein, 1983: Normal monthly wind stress over the world ocean with error estimates. *J. Phys. Oceanogr.*, **13,** 1093–1104.

Kawase, M., 1987: Establishment of deep ocean circulation driven by deep-water production. *J. Phys. Oceanogr.,* **17,** 2294–2317.

Keffer, T., 1985: The ventilation of the World's Oceans: Maps of the potential vorticity field. *J. Phys. Oceanogr.*, **15,** 509–523.

Killworth, P. D., D. B. Chelton, and R. A. De Szoeke, 1997: The speed of observed and theoretical long extratropical planetary waves. *J. Phys. Oceanogr.*, **27,** 1946–1966.

Le Traon, P.-Y., and J.-F. Minster, 1993: Sea level variability and semiannual Rossby waves in the South Atlantic subtropical gyre. *J. Geophys. Res.,* **98,** 12 315–12 326.

Levitus, S., and T. Boyer, 1994: *World Ocean Atlas 1994.* Vol. 4: *Temperature. NOAA Atlas NESDIS 4.*

McCreary, J. P., 1981: A linear stratified ocean model of the equatorial undercurrent. *Philos. Trans. Roy. Soc. London,* **298A,** 603–635.

Pedlosky, J., 1996: Vertical structure: Baroclinic quasi-geostraphic models. *Ocean Circulation Theory,* Springer-Verlag, 93–170.

Philander, S. G., 1990: *El Niño, La Niña and the Southern Oscillation.* Academic Press, 289 pp.

Phlips, P. J., 1987: A simple model of the wind-driven tropical ocean. *J. Phys. Oceanogr.*, **17,** 2003–2015.

Qiu, B., W. Miao, and P. Müller, 1997: Propagation and decay of forced and baroclinic Rossby waves in off-equatorial oceans. *J. Phys. Oceanogr.*, **27,** 2405–2417.

Rhines, P. B., and W. R. Young, 1982a: A theory for the wind-driven circulation. I: Mid-ocean gyres. *J. Mar. Res.*, **40** (Suppl), 559–596.

——, and ——, 1982b: Homogenization of potential vorticity in planetary gyres. *J. Fluid Mech.*, **122,** 347–367.

Sverdrup, H. U., 1947: Wind driven currents in a baroclinic ocean with application to the equatorial currents of the eastern Pacific. *Proc. Natl. Acad. Sci. USA,* **33,** 318–326.

White, W. B., G. A Meyers, J. R. Donguy, and S. E. Pazan, 1985: Short-term climate variability in the thermal structure of the Pacific Ocean during 1979–82. *J. Phys. Oceanogr.*, **15,** 917–935.

Young, W. R., and P. B. Rhines, 1982: A theory for the wind-driven circulation. II: Gyres with western boundary layers. *J. Mar. Res.* **40** (Suppl.), 849–872.

Zebiak, S. E., and M. A. Cane, 1987: A model El Niño–Southern Oscillation. *Mon. Wea. Rev.*, **115,** 2262–2278.